Locally-Stable Macromodels of Integrated Digital Devices for Multimedia Applications

Igor S. Stievano, *Member, IEEE*, Claudio Siviero, Ivan A. Maio, and Flavio G. Canavero, *Fellow, IEEE*

***Abstract*—This paper addresses the development of accurate and efficient behavioral models of digital integrated circuits for the assessment of high-speed systems. Device models are based on suitable parametric expressions estimated from port transient responses and are effective at system level, where the quality of functional signals and the impact of supply noise need to be simulated. A potential limitation of some state-of-the-art modeling techniques resides in hidden instabilities manifesting themselves in the use of models, without being evident in the building phase of the same models. This contribution compares three recently-proposed model structures, and selects the local-linear state-space modeling technique as an optimal candidate for the signal integrity assessment of data links. In fact, this technique combines a simple verification of the local stability of models with a limited model size and an easy implementation in commercial simulation tools. An application of the proposed methodology to a real problem involving commercial devices and a data-link of a wireless device demonstrates the validity of this approach.**

***Index Terms*—Circuit models, digital integrated circuits, input/output (I/O) buffers, signal integrity, system identification.**

I. Introduction

NOWADAYS, the design of modern high-performance electronic systems for a wide range of applications (including information and communication technology devices) requires an accurate evaluation of the system performance and implies the assessment of signal integrity and electromagnetic compatibility (EMC) effects in the early stage of the design process. In particular, the increasing data rates in the gigabit range along with the time-to-market constraints demand for accurate predictions of the time evolution of signals propagating on interconnect structures. Such predictions, that are mainly achieved by the numerical simulation of interconnecting paths, are used for detecting critical phenomena like crosstalk, time delays, or radiation that may compromise the regular operation of the system or its compliance with EMC regulations.

For these simulations, the availability of computational models of all elements of the system (i.e., digital devices, connectors, board traces and their discontinuities) is extremely important. In this framework, device models play a key role since the integrated circuits (ICs) input/output (I/O) buffers act as nonlinear dynamic terminations for the interconnects and strongly influence the shape of signals on the interconnects themselves. Besides, detailed models of real components, that are based on the internal physics of devices, turn out to be very complex and cannot be effectively used in a simulation environment. In addition, they are seldom available since they disclose information on the internal structure and technology of devices that represent confidential proprietary information of IC suppliers. Owing to this, the best way to handle IC models turns out to be the development of behavioral models that attempt to reproduce the electrical behavior of devices at their interfaces with the external circuitry; in addition, the model parameters need to be estimated from the observation of the signals at the IC interfaces.

A common approach to the behavioral modeling of IC ports is via simplified equivalent circuit representations, in which an idealized structure of the device is used to derive a simplified equivalent circuit, whose various elements account for specific static or dynamic effects. A well-known example of this structure is provided by the I/O buffer information specification (IBIS) [1], that has been established as a standard for the ports description of a digital integrated circuit, leading to a large availability of device descriptions. However, the growing complexity of recent devices and their enhanced features like pre-emphasis and specific control circuitry, demand for refinements of the basic equivalent circuits. In order to facilitate the modeling of these features, an alternate methodology based on the estimation of suitable parametric relations and circuit theory has been developed [2]–[4]. The proposed methodology is aimed at reproducing the electrical behavior of device ports, without need of technology and/or physical layout information. The advantage of this approach relies in the flexibility of the mathematical description of models with respect to the circuit representation.

The parametric relations used so far for the IC model generation belong to the class of discrete-time nonlinear auto regressive with eXtra input (NARX) parametric relations expressed in terms of gaussian or sigmoidal expansions [5]. Such models are equivalent to recurrent neural networks with one hidden layer and a linear output unit [5], [6]. This choice is based on the strength of these models to approximate the complex dynamic behavior of real systems and from the large availability of methods for parameter estimation [7], [8]. Our previous experience has shown that parametric models are accurate and efficient enough for the modeling of commercial devices for the solution of real application problems [2], [3], [9]–[11]. However, NARX relations have some inherent limitations. Mainly, 1) stability of models cannot be easily imposed *a priori* or even during the training process without impacting on model accuracy; 2) fully nonlinear optimization algorithms are required for

Manuscript received August 28, 2007; revised February 19, 2008. First published May 16, 2008; current version published November 28, 2008. This work was recommended for publication by Associate Editor P. Franzon upon evaluation of the reviewers comments.

The authors are with the Dipartimento di Elettronica, Politecnico di Torino, 10129, Torino, Italy.

Digital Object Identifier 10.1109/TADVP.2008.924214

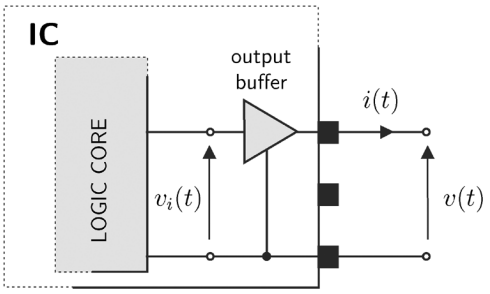

Fig. 1. Typical IC output buffer with the relevant electric variables.

the computation of model parameters and model accuracy depends on the initial guess of parameters and on local minima of the cost function; 3) higher order dynamical effects may not be readily represented by these models; 4) model estimation for real devices with multiple ports is troublesome.

In order to address the previous limitations, along with the requirement of avoiding the use of complex model structures, model representations based on composite local linear state-space models (LLSS) [12] and model representations based on the so-called echo state networks (ESN) [13], [14] are considered. The selected representations, that have been recently presented in the literature and that have several potential strengths to overcome most of the problems outlined above, are good candidates to be used for the modeling problem at hand. Preliminary results on the application of ESN and LLSS models for the behavioral modeling of digital devices are reported in [15] and [16].

This paper is organized as follows. Section II discusses the state-of-the-art model structure assumed for the behavioral characterization of IC buffers. Section III reviews the discrete-time models defined by NARX parametric relations and highlights their strengths and limitations in their application to IC modeling. Sections IV and V introduce LLSS and ESN models, including a short review of their estimation procedure. Section VI deals with the systematic analysis of the performances of the state-of-the-art NARX relations considered so far and of the proposed state-space relations in approximating the port behavior of IC devices. Finally, Section VII summarizes the results on the application of the proposed approach to a real application problem involving commercial devices and a typical mobile data-link. Summary and conclusions are given in Section VIII.

II. Behavioral Models of IC Buffers

This section shortly discusses the model structure assumed for the behavioral modeling of IC buffers. For the sake of simplicity, the following discussion is based on single-ended output buffers like the one shown in Fig. 1. The results, however, are extensible to input and supply ports and different device technologies [2], [10].

The ideal behavioral model of the output buffer in Fig. 1 would be the constitutive relation of its output port: $i = f(v, dv/dt, \ldots, v_i, dv_i/dt, \ldots)$, where i and v are the current and voltage of the output port, respectively, and v_i is any variable controlling the port logic state. However, the following time-varying two-piece model is more commonly adopted [2], since the controlling variables are not accessible from port responses only

$$i(t) = w_H(t) i_H\left(v(t), d/dt\right) + w_L(t) i_L\left(v(t), d/dt\right). \quad (1)$$

In the above relation, i_H and i_L are submodels describing the nonlinear dynamic behavior of the port in the fixed high and low logic states, respectively, and w_H and w_L are weighting signals describing state transitions and playing the same role of internal variables.

Submodels i_H and i_L are conveniently expressed as a sum of a static and a dynamic part, as follows:

$$\begin{cases} i_H\left(v(t), d/dt\right) = \overline{i}_H\left(v(t)\right) + \hat{i}_H\left(v(t), d/dt\right) \\ i_L\left(v(t), d/dt\right) = \overline{i}_L\left(v(t)\right) + \hat{i}_L\left(v(t), d/dt\right) \end{cases} \quad (2)$$

where $\overline{i}_H$ and $\overline{i}_L$ are the static characteristics of the output port in high or low logic states, respectively, and $\hat{i}_H$ and $\hat{i}_L$ are general nonlinear models accounting for the dynamic behavior of the port. The formal justification on the splitting of static and dynamic contributions is provided in [11].

The estimation of model (1) amounts to selecting a model representation for submodels $\hat{i}_H$ and $\hat{i}_L$ in (2) and to computing the model parameters. It is worth noting that the selection of the model representation along with a good algorithm for the estimation of model parameters are the most critical steps of the modeling process. In fact, once the submodels $\hat{i}_H$ and $\hat{i}_L$, and therefore i_H and i_L, are completely defined, the computation of the weighting coefficients w_H and w_L in (1) is carried out by a simple linear inversion of the model equation. This is done from voltage and current waveforms recorded during state transitions events, as suggested in [9]. The curves required for the w's computation are the port voltage and current responses computed while the driver sends a pulse, i.e., it produces a bit pattern "`010`," on a resistor and on the series connection of a resistor and a power supply battery. Finally, the last step of the modeling process amounts to translating the model equations in a simulation environment. This can be done by representing (1) and (2) in terms of an equivalent circuit and then implementing the equivalent as a SPICE-like subcircuit. The circuit interpretation of model equations is a standard procedure that is based on the use of controlled-current sources for the static contributions, and on resistors, capacitors, and controlled source elements for the dynamic parts. As an example, the SPICE-like implementation of a generic nonlinear dynamic parametric model is discussed in [9]. As an alternative, model (1) can be directly plugged into a mixed-signal simulation environment by describing model equations via hardware description languages like Verilog-AMS or VHDL-AMS.

III. NARX Parametric Relations

Recently, model representations for the dynamic parts in (2) or even for the complete submodels i_H and i_L in (1), have been sought for within the class of discrete-time NARX parametric relations. This choice arises from the large availability of methods for parameter estimation, as well as from the nice features of these models to approximate *almost any* nonlinear dynamical system [5], [19], [20]. As outlined in the Section I, NARX parametric models have been successfully applied to the modeling of input and output ports of commercial single-ended

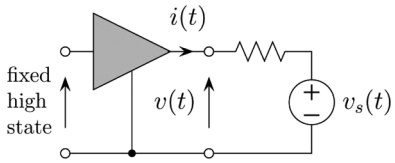

Fig. 2. Ideal setup for the estimation of a parametric model for the dynamic part $\hat{i}_H$ in (2).

complementary metal–oxide–semiconductor (CMOS) devices by means of the transient responses of their transistor-level models. The estimation of parametric models from measured transient responses is demonstrated in [3]. The extension of the methodology in order to take into account the device temperature, the power supply voltage, the power supply current drawn by buffers, as well as to model tristate devices is addressed in [2]. Finally, results on the modeling of differential low voltage differential signaling (LVDS) devices has appeared in [11].

As an example, the discrete-time NARX parametric relation for $\hat{i}_H(v, d/dt)$ is defined by the following general representation:

$$\hat{i}_H(k) = g\left(\hat{i}_H(k-1), \ldots, \hat{i}_H(k-r), v(k), v(k-1), \ldots, v(k-r)\right) \quad (3)$$

where k is the discrete-time variable, g is a parametrized nonlinear mapping, and r is the dynamical order of the model. A similar relation holds for $\hat{i}_L(v(t), d/dt)$. As already done in [2], g is expressed in terms of a sum of p sigmoidal basis functions, whose parameters are the amplitude, the position, and the spreading of each sigmoidal function.

The estimation of the model parameters in (3) is done by fitting the model responses to the so-called estimation signals, that are the port responses of the modeled device to suitable stimuli. As an example, for the dynamic part $\hat{i}_H$, the estimation signals are obtained from the ideal setup shown in Fig. 2. They correspond to the port voltage response $v(t)$ and, according to (2), to the signal $i(t) - \bar{i}_H(v(t))$. In the above setup, the port is forced in fixed high state and a voltage source designed to excite the nonlinear dynamic behavior of the device is connected to the output port. For the source v_s, noisy multilevel voltage signals composed of random steps with duration and transition times on the order of the port switching times are employed [9]. The sampled estimation signals (e.g., $v(k) = v(kT)$, T being the sampling period) are then used to fit the model response by means of standard estimation methods [7], [8]. A similar procedure is applied for the estimation of submodel $\hat{i}_L$.

NARX parametric relations turn out to be very compact, i.e., they have a dynamical order r in the range (1, 3) and are composed of a very limited number of sigmoidal units within the range (2, 10), thus leading to models with a very small size. Owing to this, the estimated models, implemented in a simulation environment, are very efficient and allow simulation speedups on the order of $(10, 1000)$ with respect to the transistor-level models of devices.

In spite of these advantages, NARX parametric relations have the following main inherent limitations.

1) The stability of models cannot be easily imposed *a-priori* and its conditioning during the training process may compromise model accuracy, as well. It is worth remarking that locally unstable models must be avoided, even if they reproduce well the reference responses used during model estimation. In fact, the numerical simulation of these models for different signal and load conditions may lead to wrong results. In order to illustrate the importance of local stability, a modeling example involving a dynamic two-terminal element driven by a voltage source is discussed. The two-terminal element is a simplified equivalent of the output port of a digital device, and is composed of the series connection of a resistor, an inductor and a capacitor. A controlled current source with a nonlinear characteristic is connected in parallel to the capacitor and the parameter values of all components are tuned to obtain a benchmark with a realistic and dynamically rich behavior. A NARX sigmoidal-based parametric model of the two-terminal element with $p = 20$ sigmoidal functions and a dynamical order $r = 3$ is generated. The model, that turns out to be locally unstable, reproduces the responses of the test case very well for a class of sources close to those used for the estimation of its parameters. However, when multilevel sources with edges faster than those used for the estimation are considered, the model gives rise to diverging and oscillating responses. An example of this behavior is shown in Fig. 3, where the current responses of the modeled two-terminal element and of its NARX model are plotted. The spurious oscillation of the NARX model are clearly visible and make it unsuitable for any practical use.

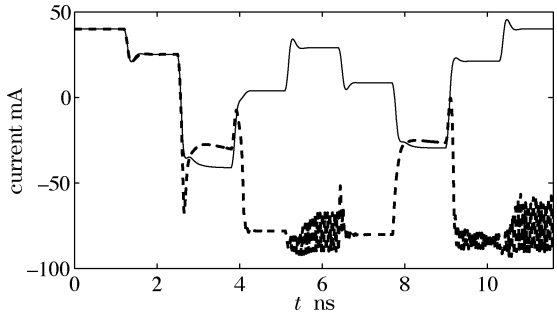

Fig. 3. Current of a two-terminal circuit element driven by an ideal voltage source producing a multilevel signal. Solid line: reference response. Dashed line: oscillating response of an unstable NARX parametric model (see text for details).

2) Fully nonlinear optimization algorithms are required for the computation of model parameters. Depending on the specific algorithm used for parameter estimation, the estimation time might be relevant. Besides, the model accuracy strongly depends on the initial guess of parameters and on local minima of the cost function.
3) Model generation for devices exhibiting a strong nonlinear behavior and possibly including higher order dynamical effects might be critical, as highlighted by the second example of Section VI.
4) Model estimation for real devices with multiple ports is troublesome and impacts the quality of estimated models. As an example, the generation of device port

models including the effects of the neighboring ports suffers from the increase of complexity of the approximation problem.

To address the inherent limitations of this class of representations, the ESN and LLSS models are considered as possible good candidates to improve the estimated models for the applications of interest.

IV. Local Linear State-Space Models

The idea underlying the LLSS modeling methodology is the approximation of the complex dynamic behavior of a nonlinear dynamical system by means of the composition of local linear models [12], [17]. The whole operating range of the system is partitioned into smaller operating regions where the system behavior is approximated by a linear state-space equation. Even if this idea is not completely new and if it has already been investigated in the past, the implementation of [12] and [17] has several strengths, including the nice feature of providing the automatic computation of local linear models as well as the generation of the weights for the local models from I/O system responses only.

As an example, for the submodel $\hat{\imath}_H(v(t), d/dt)$ of (2), a LLSS representation is defined by the following discrete-time state-space equation:

$$\begin{cases} \mathbf{x}(k) = \sum_{j=1}^{p} \rho_j\left(\mathbf{s}(k-1)\right) \\ \qquad \times \left(\mathbf{A}_j \mathbf{x}(k-1) + \mathbf{b}_j v(k-1) + \mathbf{o}_j\right) \\ \hat{\imath}_H^{(n,p)}(k) = \sum_{j=1}^{p} \rho_j\left(\mathbf{s}(k)\right)\left(\mathbf{c}_j^{\mathrm{T}} \mathbf{x}(k) + d_j v(k) + q_j\right) \end{cases} \tag{4}$$

where p is the number of local-linear models and $\rho_j(\cdot)$ is the weighting coefficient of the jth local state-space model. Each local model is defined by the state matrix $\mathbf{A}_j$, by the vectors $\mathbf{b}_j$, $\mathbf{o}_j$, and $\mathbf{c}_j$, and by the scalar coefficients d_j and q_j. Vector $\mathbf{x} = [x_1, \ldots, x_n]^{\mathrm{T}}$ defines the n internal states of the state-space relation. The argument of the weights, i.e., the scheduling vector $\mathbf{s}(k)$, corresponds to the operating point of the system and is in general a function of both input and state variables. However, in this study the simplest dependence of the type $\rho_j(v(k))$ is successfully adopted, as demonstrated in Section VI. Finally, the weight coefficients in (4) consist of normalized radial basis functions, i.e.,

$$\rho_j\left(v(k)\right) = \frac{\phi_j\left(v(k)\right)}{\sum_{i=1}^{p} \phi_i\left(v(k)\right)} \tag{5}$$

where $\phi_j(\cdot)$ is the jth radial basis function

$$\phi_j\left(\mathbf{s}(k)\right) = \exp\left(-\frac{\left\|\mathbf{s}(k) - \mathbf{t}_j\right\|^2}{\beta_j^2}\right) \tag{6}$$

whose position in the space of the system operating points is represented by the center $\mathbf{t}_j$ and whose spreading is given by the scale parameter β_j. It is worth noting that each coefficient defined by (5) varies between zero and one and the sum of all coefficients is forced to be one at each operating point of the system.

The determination of the model parameters defined above in (4)–(6) requires the solution of a nonlinear nonconvex approximation problem, whose solution requires a modified version of the Levenberg–Marquardt (LM) iterative method as proposed by [12]. This modified algorithm has the following two good properties: 1) it can handle the nonuniqueness of a state-space representation that may cause ill-conditioning of matrices during model estimation; 2) the parameter initialization is carried out by means of a deterministic procedure, thus avoiding the dependence of the estimated model to the initial guess of parameters. In addition, the initial guess of parameters refers to a single global stable linear model and is computed by means of the application of an efficient subspace identification method [23], [24], that provides also the automatic computation of the number of internal state variables, i.e., the size of vector $\mathbf{x}$ in (4). It is worth to remark that in the proposed implementation of the algorithm, no additional constraints are included to enforce stable models during the training phase, and stability is only verified a posteriori. However, for the modeling problems at hand, the proposed approach has always have been verified to generated stable models.

The algorithm for the estimation of the parameters of the LLSS model defined by (4)–(6) is outlined by the following pseudocode with embedded comments. A Matlab-like notation is used to indicate matrices and their elements.

1) Generate the estimation and validation waveforms $v_e(t)$, $i_e(t)$, $v_v(t)$, and $i_v(t)$ [the waveforms are the voltage and current responses of the setup of Fig. 2 to two different perturbation signals $v_s(t)$].
2) Define the estimation and validation sequences
   $ts = [0 : \mathrm{numsamples} - 1] * T;$
   $u = \mathrm{interp}(v_e(t), ts);\ y = \mathrm{interp}(i_e(t), ts) - \overline{\imath}(u)$
   $uval = \mathrm{interp}(v_v(t), ts);\ yval = \mathrm{interp}(i_v(t), ts) - \overline{\imath}(uval)$
   [$\overline{\imath}(\cdot)$ is the model static characteristic; the estimation and validation waveforms are sampled with sampling pitch T in order to define the samples of the system inputs and outputs that are used for the estimation of the model parameters and for the model validation].
3) Estimate the model order n and the starting values for the model parameters $\mathbf{A}_j$, $\mathbf{b}_j$, $\mathbf{o}_j$, $\mathbf{c}_j$, d_j, q_j, $\mathbf{t}_j$, and β_j [the order and the starting parameter values are estimated by applying a subspace state space identification (4SID) method to the estimation sequences (e.g., see [23] and [24]); the Matlab routine `N4SID` of the Matlab System Identification Toolbox provides a ready-to-use implementation of 4SID methods].
4) For $p = 1 : pmax$ do
   a) estimate the parameter of the LLSS model $\hat{\imath}^{(n,p)}$ that is defined by p linear submodels [the parameters are estimated by means of the modified LM algorithm [12]; the algorithm is initialized with the starting parameter values];
   b) compute the response of the model to $uval : ymodval = \hat{\imath}^{(n,p)}(uval)$;
   c) compute the mean square error of the model: $MSE(p) = \|ymodval - yval\|_2$.

5) Find $q = min_p(MSE(p))$ and output $\hat{i}^{(n,q)}$ as the estimated model.

V. Echo State Networks

This section briefly discusses the alternate class of models defined by the ESNs. This class of models is described by a nonlinear discrete-time state-space equation that is able to approximate a wide class of nonlinear dynamical systems. As an example, for the dynamic part $\hat{\imath}_H(v(t), d/dt)$ of (2), a ESN parametric representation writes

$$\begin{cases} \mathbf{x}(k) = \mathbf{f}\left(\mathbf{A}\mathbf{x}(k-1) + \mathbf{b}v(k-1)\right) \\ \hat{\imath}_H(k) = \mathbf{c}^T\left[\mathbf{x}^T(k), v(k)\right]^T \end{cases} \tag{7}$$

where vector $\mathbf{x} = [x_1, \ldots, x_N]^T$ collects the N internal state variables. Typical values of N are in the range [20,500] and the nonlinear multivariate mapping $\mathbf{f}$ consists of the collection of sigmoidal functions, i.e., $\mathbf{f} = [\tanh(\cdot), \ldots, \tanh(\cdot)]^T$. The parameters of the model are the square matrix $\mathbf{A}$ and vectors $\mathbf{b}$ and $\mathbf{c}$.

Although the parameters estimation requires in principle the solution of a fully nonlinear optimization problem, the adopted ESN methodology amounts to compute only the weights of the network-to-output connections, i.e., the parameters in vector $\mathbf{c}$, and this leads to the solution of a linear least squares problem. The remaining parameters, i.e., matrix $\mathbf{A}$ and vector $\mathbf{b}$, are defined *a priori* in a way that allows the inclusion in the model of a large number of randomly generated dynamics, possibly including those of the original system under modeling. Matrix $\mathbf{A}$ is chosen to satisfy the "echo state" property, which means that for each input sequence, model (7) must present a unique sequence of state variables. In order to fulfill the "echo state" requirement, the square matrix $\mathbf{A}$ is chosen to have a spectral radius ρ smaller than one (e.g., $\rho = (0.7, 0.99)$). It can be easily proven that the above assumption, along with the choice of the tanh function in the nonlinear mapping $\mathbf{f}$, leads to locally stable ESN models. Within the many possible choices for $\mathbf{A}$, that have not been completely investigated yet, the solution proposed by [18] is adopted, whereby matrix $\mathbf{A}$ is generated as a sparsely and randomly connected matrix, whose elements are independent random variables that have a certain (high) probability to be zero (e.g., 95%), and the complementary probability, named connectivity χ, to be $\pm a$, where a is real positive number. The number a is then computed to enforce the spectral radius ρ to the desired value. This choice satisfies a sufficient and hence restrictive condition for the "echo state" property. Better solutions allowing a higher degree of freedom exist and are currently under investigation [21].

Once matrix $\mathbf{A}$ is determined, vector $\mathbf{b}$ is chosen to avoid the saturation of the sigmoidal functions and vector $\mathbf{c}$ is computed by recasting the model equation in terms of the solution of a standard linear least squares problem, as detailed in the following. For the sake of simplicity, the discussion is based on submodel $\hat{\imath}_H$ only. For this case, the input and output estimation sequences obtained from the setup of Fig. 2, i.e., the port voltage sequence $\{v(k)\}$, $k = 1 \ldots K$ and the corresponding output sequence $i(k) - \overline{\imath}_H(v(k))$, are used to rewrite the model (7) as follows:

$$\begin{bmatrix} \hat{\imath}_H(k_0+1) \\ \hat{\imath}_H(k_0+2) \\ \vdots \\ \hat{\imath}_H(K) \end{bmatrix} = \begin{bmatrix} i(k_0+1) - \overline{\imath}_H\left(v(k_0+1)\right) \\ i(k_0+2) - \overline{\imath}_H\left(v(k_0+2)\right) \\ \vdots \\ i(K) - \overline{\imath}_H\left(v(K)\right) \end{bmatrix} = \begin{bmatrix} \mathbf{x}^T(k_0+1) & v(k_0+1) \\ \mathbf{x}^T(k_0+2) & v(k_0+2) \\ \vdots & \vdots \\ \mathbf{x}^T(K) & v(K) \end{bmatrix} \mathbf{c} \tag{8}$$

where the first k_0 elements are eliminated to avoid the effects of the initial *free* evolution of states. Vector $\mathbf{c}$ can be thus computed by means of (8) and standard linear projection techniques.

In summary, ESN designed as outlined in this section have several good features: they are stable by construction, they rely on a simple linear estimation algorithm, and they effectively approximate the nonlinear dynamic behavior of complex and high-order dynamical systems.

The algorithm for the estimation of the parameters of the ESN model defined by the (7) is outlined by the following pseudocode with embedded comments. Also for this case, a Matlab-like notation is used to indicate matrices and their elements.

1) Generate the estimation and validation waveforms $v_e(t)$, $i_e(t)$, $v_v(t)$, and $i_v(t)$ [the waveforms are the voltage and current responses of the setup of Fig. 2 to two different perturbation signals $v_s(t)$].
2) Define the estimation and validation sequences
   $ts = [0 : \text{numsamples} - 1] * T$;
   $u = \text{interp}(v_e(t), ts)$; $y = \text{interp}(i_e(t), ts) - \overline{\imath}(u)$.
   $uval = \text{interp}(v_v(t), ts)$; $yval = \text{interp}(i_v(t), ts) - \overline{\imath}(uval)$.
3) For $N = N_{\min} : N_{\max}$ do
   a) estimate the parameter of the ESN model $\hat{\imath}^{(N)}$ [13], [14], [18]
      - define $A_1 = \text{rand}(N)$; $\rho_2 = \max(\text{eig}(A_2))$ [ρ_2 is the spectral radius of the random auxiliary matrix A_2].
      - process A_1 to obtain a new matrix A_2 with entries {0,1,−1} only [the entries of A_1 are forced to be zero with a probability $P = (1 - \chi)$(e.g., $\chi = 5\%$, $P = 95\%$). The remaining nonzero positive (negative) entries are forced to be 1 (−1)]
      - assign ρ (e.g., 0.9) and define $A = (\rho/\rho_2) * A_2$ [The ESN state-space matrix A is thus forced to have entries $\{0, -a, a\}$, $a = (\rho/\rho_2)$ with a spectral radius ρ]
      - generate the vector $\mathbf{b}$ of (7) [vector $\mathbf{b}$ is a random vector with entries that limit the argument of the multivariate function $\mathbf{f}$ of (7) to be within the range (-0.9, 0.9), thus avoiding the saturation of the tanh functions composing $\mathbf{f}$]
      - rewrite the model equation in terms of the linear least squares problem (8) and compute the vector $\mathbf{c}$

b) compute the response of the model to $uval : ymodval = \hat{i}^{(N)}(uval)$;
c) compute the mean square error of the model: $\mathrm{MSE}(N) = \|ymodval - yval\|_2$.

4) Find $N_{\mathrm{best}} = \min_N(\mathrm{MSE}(N))$ and output $\hat{i}^{(N_{\mathrm{best}})}$ as the estimated model.

VI. Performance Assessment

In this section, the methodology for the generation of IC macromodels based on the different parametric relations discussed in this paper is applied to a commercial device of interest. The example device is a 8-bit bus transceiver with four independent buffers produced by Texas Instruments (model name SN74ALVCH16973, power supply voltage VDD $= 1.8$ V). The example device operates at 167 Mbps, i.e., the bit time is 6 ns. The HSPICE transistor-level description is available from the official website of the vendor, and the simulations of this model will be used in the following both for the generation of the estimation signals and as the reference curves for the model validation. In this study, two different examples are considered. They are based on the same device, but they differ for the inclusion or not of the IC package information in the transceiver description and, consequently, in the estimated behavioral model. The lumped circuit equivalent of the IC package is provided by the supplier as well. For both examples, the behavioral models expressed in terms of sigmoidal-based NARX relations, LLSS and ESN models are estimated. The figures of their performances in terms of accuracy, efficiency, model stability, and estimation time are compared.

Example 1: In the first example, the proposed modeling methodology is applied to the characterization of the silicon part of the output port of the example device. No package information is included in the reference transistor-level description of the transceiver. As an example, Fig. 4 shows the output port voltage $v(t)$ and current $i(t)$ responses used for the estimation of submodel $\hat{i}_H$. The port responses are computed, as shown in the ideal setup of Fig. 2, where the driver is forced in fixed high output state and a noisy multilevel signal is used for the voltage source $v_s(t)$. Similar curves can be obtained for the alternate submodel $\hat{i}_L$.

For this example, different models accounting for the dynamic parts $\hat{i}_H$ and $\hat{i}_L$ are estimated. NARX-based models are illustrated first: they are expressed in terms of sigmoidal expansions obtained by means of the application of either static [7] or recurrent [8] estimation algorithms. All these models have dynamic order $r = 2$ and a number of basis functions selected by the estimation algorithm in the range (3,10). LLSS-based models are then obtained by means of the algorithm described in Section IV. These models turn out to be composed of a number of local linear models in the range (2,4) and three state variables. Lastly, ESN-based models are estimated as outlined in Section V, and show a number of internal states in the range (10,200). The specific parameters of this class, i.e., the spectral radius and the connectivity, are set to $\rho = 0.85$ and $\chi = 5\%$, respectively.

The accuracy of the models estimated by means of the three above-mentioned techniques is quantified by computing the mean squares error (MSE) between the model and the real

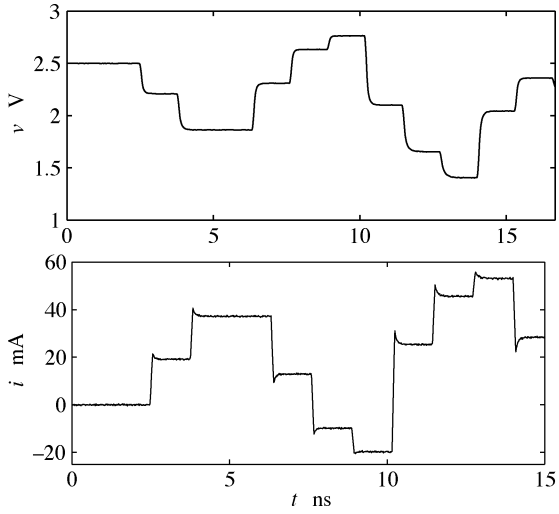

Fig. 4. Device output port voltage $v(t)$ and current $i(t)$ responses computed for the setup in Fig. 2. The driver is replaced by the transistor-level description of Example 1 and a multilevel signal is used for the voltage source $v_s(t)$.

device responses, for a validation test. In order to simplify the discussion, the validation test consists of the HSPICE simulation of the setup shown in Fig. 2, where the voltage source is again a multilevel signal but different from the one used for the estimation of model parameters. Also, without loss of generality, the comments are limited to model responses in fixed high state. The CPU time required by the estimation of model parameters is also reported, as an additional index intended to quantify the cost of model generation. The model efficiency is included in the comparison and is quantified by means of the speedup obtained by running the different models. The speedup parameter is the ratio of the simulation time required by the different models and the simulation time required by the reference transistor-level model to perform the transient analysis of the validation test. Finally, model stability is assessed by computing the eigenvalues of the linearized model (1). The eigenvalues are computed for each time step of the HSPICE simulations of the validation test, as suggested by [22].

Table I collects the main figures of the estimated models illustrated above. The model size of column three represents the number of basis functions for the NARX relations, the number of local linear models for the LLSS case, and the number of internal states for ESN case. The last three columns report the performance of the estimated models quantified by the MSE index, by the CPU time required for model estimation and by the simulation speedup.

The figures of Table I highlight that all the representations considered in this study lead to models with comparable MSE values. This remark is also confirmed by the validation curves of Fig. 5, that compares the reference output port current response and the response of model 1. The validation responses of the remaining models are not reported, since they are almost indistinguishable from those of Fig. 5. It is also worth noting that ESN-based models with a number of states larger than 120, do not lead to improved accuracy. Conversely, the accuracy of models with a small number of states ($N \leq 30$) strongly depends on the different runs of the estimation algorithm. This is

TABLE I
MODELS PERFORMANCE: ACCURACY, ESTIMATION TIME, AND SPEED-UP OF THE DIFFERENT MODELS CONSIDERED IN EXAMPLE 1 (SEE TEXT FOR DETAILS)

#	Model type	Complexity (model size)	Mean square error (MSE)	Estimation time	Efficiency (speed-up)
1	NARX with static estimation	$p = 5$	1.1e-8	2.4 s	25x
2	NARX with recurrent estimation	$p = 5$	2.9e-8	58 s	25x
3	LLSS	$p = 3$	1.0e-8	11 s	20x
4	ESN	$N = 30$	1.5e-8	0.1 s	8x
5	ESN	$N = 60$	1.8e-8	0.2 s	4x
6	ESN	$N = 120$	7.6e-8	0.5 s	0.5x

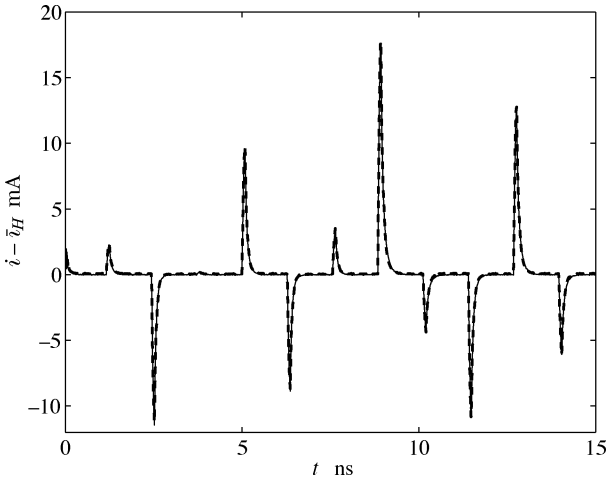

Fig. 5. Dynamic part of the port current responses for Example 1 validation test. The curves refer to an HSPICE simulation of the ideal setup of Fig. 2, where the voltage source $v_s(t)$ produces a staircase signal different from the one used for the model estimation. Solid thin line: reference, dashed thick line: model 1.

due to the fact that matrix $\mathbf{A}$ has a very limited number of randomly generated states that might not include a sufficient variety of dynamic features needed to mimic the reference behavior of the device. As a final remark on model accuracy, both static or recurrent algorithms for the estimation of NARX relations provide similar results.

From Table I, it is also worth noting that the CPU time required for the estimation of ESN models is much less than the time required for the estimation of NARX or LLSS models, since ESN relies on the solution of a linear least squares problem, while NARX and LLSS require the solution of nonlinear optimization problems.

Fig. 6 shows the eigenloci of the linearized model (1) for the dynamic part of i_H defined by the three different parametric relations used in models 1, 3, and 4, respectively. Fig. 6(a) refers to ESN-based models and shows that all the eigenvalues lie within the unitary circle, as expected because these models are stable by construction. Similarly, Fig. 6(b), referring to LLSS-based models, shows a good behavior of eigenvalues and allows the *a posteriori* verification of the model stability. On the other hand, Fig. 6(c), referring to NARX parametric models, indicates that several eigenvalues lie outside the unitary circle, and confirms that potential dynamic instability can arise, since no constraint on the model stability is imposed during model estimation.

The last column of Table I reports the speedup introduced by the HSPICE implementations of the estimated models. From comparison of values in this column, it is clear that both NARX-based and LLSS-based models, that are generally smaller in size, show the best efficiency. However, for devices of interest like the one used in this example, ESN-based models with a limited number of internal states (e.g., $N = 30$) provide accurate results with the inherent advantage of having always locally stable models and a reasonable penalty in terms of model efficiency.

Example 2: In the second example, the modeling process is repeated for a device including the IC package information. Thus, it is expected to deal with higher order dynamical effects introduced by the package parasitics components.

The same set of experiments devised for the Example 1 have been carried out and the main results can be summarized as follows. Even if NARX models leading to a reasonably good accuracy can be still generated, the model quality for devices with richer dynamics strongly depends on the initialization of model parameters for both the static and the recurrent estimation algorithms. This can be clearly appreciated from Fig. 7, that compares the reference output port current response and the responses of ten different NARX models. Furthermore, NARX parametric relations have the same potential instability highlighted in the previous example. On the contrary, ESN and LLSS techniques provide stable models and require one single run of the estimation algorithm to obtain the results shown in Fig. 8. From Fig. 8, it is also clear that LLSS models offer improved accuracy in reproducing the reference responses of the example device.

Table II collects the main figures of the estimated models for this second example. The structure of this table is the same of Table I. As already seen from the curves of Figs. 7 and 8 the

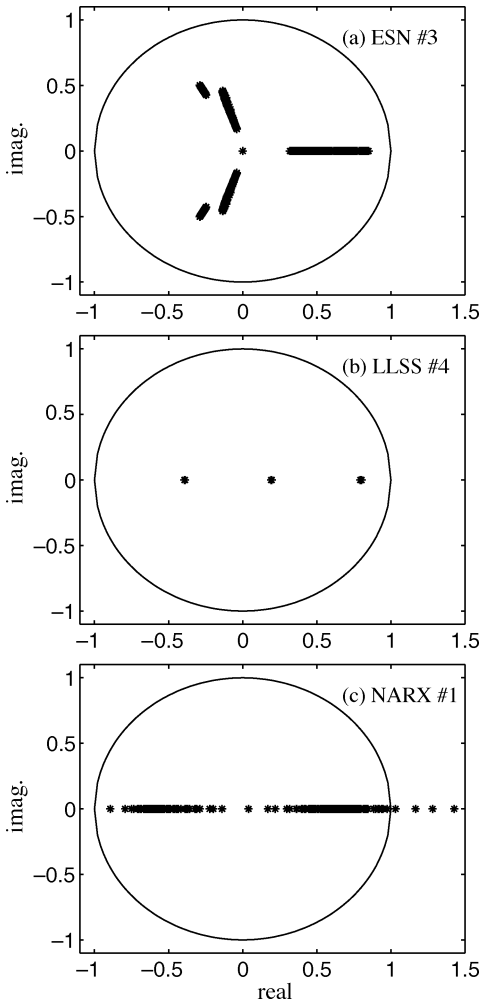

Fig. 6. Eigenvalues of the linearized parametric relations used in model 3 (panel a), 4, (panel b), and 1 (panel c) for the dynamic part $\hat{\imath}_H$ in (2). The eigenvalues are computed at each point explored during the transient simulation of Example 1 validation test.

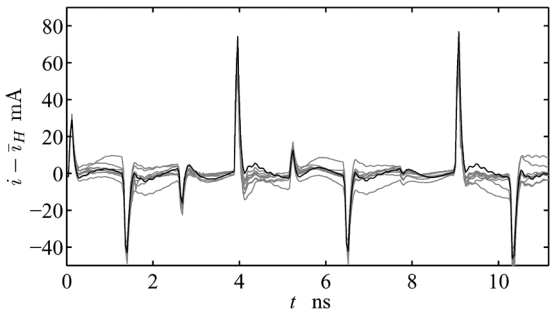

Fig. 7. Dynamic part of the port current responses for Example 2 validation test. The curves refer to an HSPICE simulation of the ideal setup of Fig. 2, where the voltage source $v_s(t)$ produces a staircase signal different from the one used for the model estimation. Solid black line: reference, solid gray lines: ten different models based on NARX parametric relations (see text).

performance indexes of Table II confirm that LLSS models offer improved accuracy and good efficiency.

Furthermore, LLSS models address all the critical issues outlined in the Introduction. In fact, they lead to locally stable models, their estimation relies on a deterministic procedure and

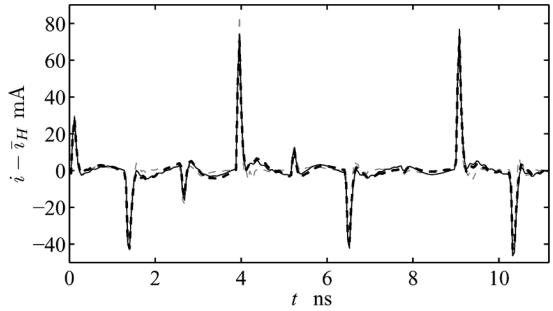

Fig. 8. Dynamic part of the port current responses for Example 2 validation test. The curves refer to an HSPICE simulation of the ideal setup of Fig. 2, where the voltage source $v_s(t)$ produces a staircase signal different from the one used for the model estimation. Solid black line: reference, dashed gray line: ESN-based model, $N = 30$; dashed black line: LLSS-based model (see text).

they can be effectively used to model devices exhibiting higher order dynamic effects. In addition, the state-space nature of the model representation facilitates the application of this approach to the modeling of devices with multiple inputs.

VII. Application

In this section, the LLSS modeling methodology, that has been demonstrated to perform best for IC modeling, is applied to the characterization of two commercial devices involved in a real communication link. The idealized structure of the link is shown in Fig. 9. It represents a RF-to-digital communication link of a wireless device and consists of a driver IC (left side) communicating with a receiver IC (right side) via a distributed interconnect, and energized by a common power supply network. A high-speed CMOS single-ended transceiver ($V_{DD} = 1.8$ V) is used for both active devices in the figure; their transistor-level description compatible with the Mentor Graphics Eldo-SPICE was available. The interconnect is a 3-cm-long MCM land, that is modeled as an ideal transmission line whose parameters are obtained from the information on the geometry of the structure and on the substrate information (the characteristic impedance is $Z_c = 100\,\Omega$ and the per-unit-length capacitance is $C = 5$ pF/m). The power supply network is modeled by a lumped equivalent and no transitions or junctions are included in the transmission path, for the sake of simplicity. In the example test case considered in this application, the IC driver produces a data pattern composed of a 50-bit-long sequence with a bit and rise time of 5 ns and 500 ps, respectively.

Specialized macromodels for the driver and receiver of Fig. 9 are estimated by means of the techniques illustrated in Sections III–V. The model structures adopted in this section are more complex than those discussed in Section II and used in validations of Section VI. In fact, the effects of the power-supply and ground voltage fluctuations need to be included, thus interpreting each device as a four-port instead of a simple input-output element. Details of this extension were already discussed in [2]; here, it is simply mentioned that, for the driver case, the inclusion of the power supply voltage leads to a two-piece model structure like (1) for both the output and the supply port current, where each submodel like i_H and i_L includes an additional input accounting for the supply voltage variable. The LLSS models computed for this application

TABLE II
MODELS PERFORMANCE: ACCURACY, ESTIMATION TIME AND SPEED-UP OF THE DIFFERENT MODELS OBTAINED FOR EXAMPLE 2 (SEE TEXT FOR DETAILS)

#	Model type	Complexity (model size)	Mean square error (MSE)	Estimation time	Efficiency (speed-up)
1	NARX with static estimation	$p = 6 \div 10$	3.9e-6 ÷ 2.3e-5	1.4 ÷ 21 s	19÷25x
2	NARX with recurrent estimation	$p = 4 \div 10$	1.4e-5 ÷ 2.9e-5	59 ÷ 186 s	25x
3	LLSS	$p = 4$	1.1e-6	14 s	19x
4	ESN	$N = 30$	8.3e-6	0.05 s	8x
5	ESN	$N = 60$	1.3e-5	0.1 s	4x
6	ESN	$N = 120$	5.4e-5	0.25 s	0.5x

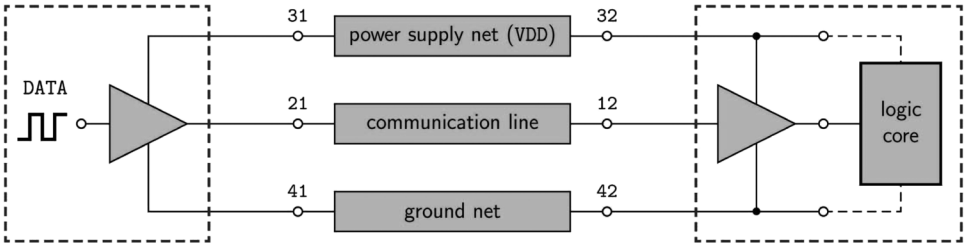

Fig. 9. Structure of the application data-link considered in Section VII.

example turn out to be composed of $p = 4$ local-linear models and $n = 3$ internal states.

In order to assess the accuracy and the efficiency of the proposed models in predicting the transient voltage waveforms, the complete structure of Fig. 9 is simulated and the results of the reference transistor-level descriptions and of the LLSS macromodels are compared.

As a first test, Figs. 10 and 11 show the comparison between the reference and the predicted functional voltage signals at the near- and far-end of the system interconnect, respectively. For an adequate appreciation of the details, the figures show only a segment of the complete 50-bit long sequence. This comparison highlights the very good correlation between the reference responses and the predicted ones, and confirms the accuracy of the proposed models in reproducing the functional signals of a high-performance interconnect. It is also worth noting that the LLSS macromodels provide accurate timing information; in fact, the timing error computed as the maximum delay between the reference and the predicted curves in crossing the 0.9-V threshold turns out to be always less than 2% of the bit time.

As a second test, Fig. 12 shows a comparison of the reference and predicted fluctuations of the supply voltage v_{31}, and indicates a good agreement between the two. This result confirms the validity of the LLSS predictions for the assessment of power-bounce analysis of data-transmission systems.

Finally, Table III collects the CPU time required by the simulation of the structure of Fig. 9 where the devices are either represented by the reference transistor-level models of devices or by the proposed macromodels. From this comparison, it is worth to remark that the LLSS macromodels can be effectively

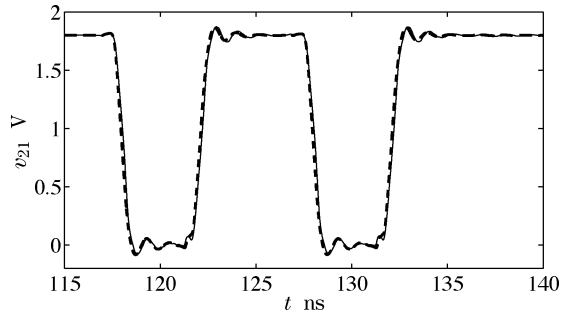

Fig. 10. Voltage waveform v_{21} at the driver output port of Fig. 9. Solid line: reference. Dashed line: prediction via LLSS macromodels.

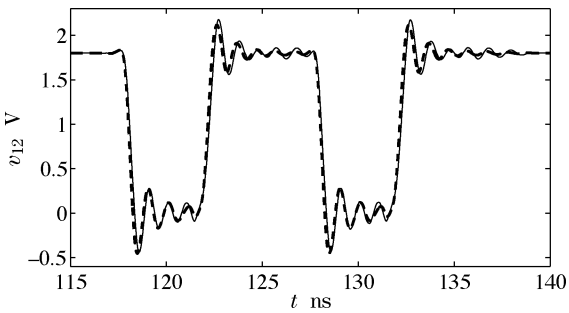

Fig. 11. Voltage waveform v_{12} at the receiver input port of Fig. 9. Solid line: reference. Dashed line: prediction via LLSS macromodels.

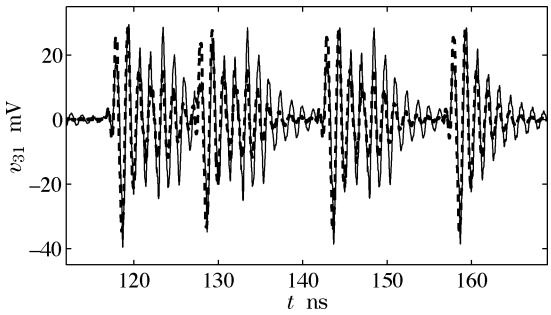

Fig. 12. Fluctuations of the voltage v_{31} at the driver power-supply port of Fig. 9. Solid line: reference. Dashed line: prediction via LLSS macromodels.

TABLE III
CPU TIME REQUIRED BY THE SIMULATION OF THE SETUP OF Fig. 9 (SEE TEXT FOR DETAILS)

Device models	Simulation time
Transistor-level (Mentor Graphics Eldo-SPICE)	36 min 26 sec
LLSS Macromodels	1 min 45 sec

used to handle the complexity of realistic structures. In fact, they allow a simulation speedup of at least $30x$ with respect to the transistor-level models.

VIII. CONCLUSION

This paper deals with the generation of IC behavioral models for the assessment of signal integrity and electromagnetic compatibility effects in high-speed digital systems. The adopted models belong to the class of discrete-time parametric relations; they are estimated form port voltage and current responses only, and can be readily implemented in any circuit simulation environment. Different possible representations based on state-space relations have been thoroughly discussed above, and their performances assessed to overcome the inherent limitations of the state-of-the-art parametric relations used so far. This study highlights that LLSS model representations provide a very good compromise between model accuracy and efficiency and seem to be the best candidate for modeling the problem at hand. LLSS-based models lead to locally stable models and their estimation relies on a deterministic procedure. Besides, they have been proven to account for the complex dynamical behavior of real devices and can be effectively used to solve real application problems.

ACKNOWLEDGMENT

The authors would like to thank A. Arslan of Nokia Research Center (NRC) for suggesting the data link structure and for allowing C. Siviero during his visit to NRC, to run the buffers models of our application example. C. Siviero would like to acknowledge the hospitality at NRC during his doctoral studies.

REFERENCES

[1] I/O Buffer information specification (IBIS) Ver. 4.1 [Online]. Available: http://www.eigroup.org/ibis/ibis.htm Jan. 2004
[2] I. S. Stievano, I. A. Maio, and F. G. Canavero, "$\mathrm{M}\pi log$ Macromodeling via parametric identification of logic gates," *IEEE Trans. Adv. Packag.*, vol. 27, no. 1, pp. 15–23, Feb. 2004.
[3] I. S. Stievano, I. A. Maio, and F. G. Canavero, "Behavioral models of I/O ports from measured transient waveforms," *IEEE Trans. Instrum. Meas.*, vol. 51, no. 6, pp. 1266–1270, Dec. 2002.
[4] B. Mutnury, M. Swaminathan, and J. P. Libous, "Macromodeling of nonlinear digital I/O drivers," *IEEE Trans. Adv. Packag.*, vol. 29, no. 1, pp. 102–113, Feb. 2006.
[5] J. Sjöberg *et al.*, "Nonlinear black-box modeling in system identification: A unified overview," *Automatica*, vol. 31, no. 12, pp. 1691–1724, 1995.
[6] S. Haykin, *Neural Networks—A Comprehensive Foundation*. Englewood Cliffs, NJ: Prentice Hall, 1999.
[7] M. T. Hagan and M. Menhaj, "Training feedforward networks with the marquardt algorithm," *IEEE Trans. Neural Networks*, vol. 5, no. 6, pp. 989–993, Nov. 1994.
[8] Y. H. Fang, M. C. E. Yagoub, F. Wang, and Q. J. Zhang, "A new macromodeling approach for nonlinear microwave circuits based on recurrent neural networks," in *Proc. 2000 IEEE MTT-S Int. Microw. Symp.*, 2000, vol. 2, pp. 883–886.
[9] I. S. Stievano, F. G. Canavero, and I. A. Maio, "Parametric macromodels of digital I/O ports," *IEEE Trans. Adv. Packag.*, vol. 25, no. 2, pp. 255–264, May 2002.
[10] I. S. Stievano, I. A. Maio, F. G. Canavero, and C. Siviero, "Parametric macromodels of differential drivers and receivers," *IEEE Trans. Adv. Packag.*, vol. 28, no. 2, pp. 189–196, May 2005.
[11] I. S. Stievano, I. A. Maio, F. G. Canavero, and C. Siviero, "Reliable eye-diagram analysis of data links via device macromodels," *IEEE Trans. Adv. Packag.*, vol. 29, no. 1, pp. 31–38, Feb. 2006.
[12] V. Verdult, L. Ljung, and M. Verhaegen, "Identification of composite local linear state-space models using a projected gradient serch," *Int. J. Control*, vol. 65, no. 16/17, pp. 1385–1398, 2002.
[13] H. Jaeger, "Adaptive nonlinear system identification with echo state networks," in *Advances in Neural Information Processing Systems*, S. T. S. Becker and K. Obermayer, Eds. Cambridge, MA: MIT Press, 2003, pp. 593–600, 2002.
[14] M. Salmen and P. G. Ploger, "Echo state networks used for motor control," in *Proc. Int. Conf. Robotics Automat.*, Apr. 18–22, 2005, pp. 1953–1958.
[15] I. S. Stievano, C. Siviero, I. A. Maio, and F. G. Canavero, "Guaranteed locally-stable macromodels of digital devices via echo state networks," in *Proc. 15th Topical Meeting Electrical Performance Electronic Packag.*, Scottsdale, AZ, Oct. 23–25, 2006, pp. 65–68.
[16] I. S. Stievano, C. Siviero, F. G. Canavero, and I. A. Maio, "Composite local-linear state-space models for the behavioral modeling of digital devices," in *Proc. 2007 IEEE Instrum. Measurement Technol. Conf.*, Warsav, Poland, May 1–3, 2007.
[17] V. Verdult, "Nonlinear system identification: A state-space approach," Ph.D. dissertation, Univ. Twente, Twente, The Netherlands, Mar. 2002.
[18] H. Jaeger, The Echo State Approach to Analyzing and Training Recurrent Neural Networks GMD—German National Research Institute for Computer Science, GMD Report 148, 2001.
[19] L. Ljung, *System Identification: Theory for the User*. Englewood Cliffs, NJ: Prentice-Hall, 1987.
[20] W. Maass, T. Natschälager, and H. Markram, "Real-time computing without stable state: A new framework for neural computation based on perturbation," *Neural Computat.*, vol. 14, no. 11, pp. 2531–2560, 2002.
[21] M. Buehener and P. Young, "A tighter bound for the echo state property," *IEEE Trans. Neural Networks*, vol. 17, no. 3, pp. 820–824, May 2006.
[22] C. Alippi and V. Piuri, "Neural modeling of dynamic systems with nonmeasurable state variables," *IEEE Trans. Instrum. Measurem.*, vol. 48, no. 6, pp. 1073–1080, Dec. 1999.
[23] P. van Overschee and B. DeMoor, *Subspace Identification of Linear Systems: Theory, Implementation, Applications*. Norwell, MA: Kluwer, 1996.
[24] M. Verhaegen, "Identification of the deterministic part MIMO state space models geven in innovations form from input-output data," *Automatica*, vol. 30, pp. 71–74, 1994.

Igor S. Stievano (M'98) received the Laurea degree and the Ph.D. degree in electronic engineering from the Politecnico di Torino, Torino, Italy, in 1996 and 2001, respectively.

Currently, he is an Assistant Professor of Circuit Theory with the Dipartimento di Elettronica, Politecnico di Torino. His research interests are in the field of electromagnetic compatibility, where he works on the macromodeling of linear and nonlinear circuit elements with specific application to the behavioral characterization of digital integrated circuits and linear junctions for the assessment of signal integrity and electromagnetic compatibility effects.

Claudio Siviero received the Laurea degree in electronic engineering from the Politecnico di Torino, Torino, Italy, in 2003.

Currently, he is a Researcher with the Dipartimento di Elettronica, Politecnico di Torino. His research interests are in the field of electromagnetic compatibility, where he works on the macromodeling of logic devices for the assessement of signal Integrity effects in high-speed digital systems.

Ivan A. Maio received the Laurea degree and the Ph.D. degree in electronic engineering from the Politecnico di Torino, Torino, Italy, in 1985 and 1989, respectively.

Currently, he is a Professor of Circuit Theory with the Dipartimento di Elettronica, Politecnico di Torino. His research interests are in the fields of electromagnetic compatibility and circuit theory, where he works on line modeling, and linear and nonlinear circuit modeling and identification.

Flavio G. Canavero (F'07) received his electronic engineering degree from Politecnico (Technical University), Torino, Italy, and the Ph.D. degree from the Georgia Institute of Technology, Atlanta, in 1986.

Currently, he is a Professor of Circuit Theory with the Department of Electronics, Politecnico di Torino. His research interests include signal integrity and EMC design issues, interconnect modeling, black-box characterization of digital integrated circuits, EMI, and statistics in EMC. He is Chair of URSI Commission E, Editor of the Practical Papers Section of the EMC Newsletters.

He was the Editor-in-Chief of IEEE TRANSACTIONS ON ELECTROMAGNETIC COMPATIBILITY. He was an organizer of two IEEE Workshops in 2007 (Signal Propagation on Interconnects and European Systems Packaging Workshop